Geochemistry Geophysics Geosystems G3
AN ELECTRONIC JOURNAL OF THE EARTH SCIENCES
Published by AGU and the Geochemical Society

Article
Volume 10, Number 4
9 April 2009
Q04009, doi:10.1029/2008GC002292
ISSN: 1525-2027

Tsunami modeling of a submarine landslide in the Fram Strait

Christian Berndt
Leibniz Institute of Marine Sciences at University of Kiel (IFM-GEOMAR), Wischhofstrasse 1-3, D-24148 Kiel, Germany (cberndt@ifm-geomar.de)

Also at National Oceanography Centre, European Way, Southampton SO14 3ZH, UK

Sascha Brune
GeoForschungsZentrum Potsdam, Telegrafenberg E3, D-14473 Potsdam, Germany

Euan Nisbet
Department of Earth Sciences, Royal Holloway University of London, Egham TW20 0EX, UK

Jochen Zschau and Stephan V. Sobolev
GeoForschungsZentrum Potsdam, Telegrafenberg E3, D-14473 Potsdam, Germany

[1] The present geological setting west of Svalbard closely parallels the situation off mid-Norway after the last glaciation, when crustal unloading by melting of ice induced very large earthquakes. Today, on the modern Svalbard margin, increasing bottom water temperatures are destabilizing marine gas hydrates, which are held in continental margin sediments consisting of interlayered contourite deposits and glacigenic debris flows. Both unloading earthquakes and hydrate failure have been identified as key factors causing several megalandslides off Norway during early Holocene deglaciation. The most prominent event was the Storegga Slide 8200 years B.P. which caused a tsunami up to 23 m high on the Faroe and Shetland islands. Here we show by numerical tsunami modeling that a smaller submarine landslide west of Svalbard, 100 m high and 130 km wide, would cause a tsunami capable of reaching northwest Europe and threatening coastal areas. A tsunami warning system based on tiltmeters would give a warning time of 1–4 h.

Components: 4219 words, 7 figures, 2 tables.

Keywords: global change; tsunamis; submarine landslides.

Index Terms: 4564 Oceanography: Physical: Tsunamis and storm surges; 3070 Marine Geology and Geophysics: Submarine landslides.

Received 20 October 2008; **Revised** 14 January 2009; **Accepted** 25 February 2009; **Published** 9 April 2009.

Berndt, C., S. Brune, E. Nisbet, J. Zschau, and S. V. Sobolev (2009), Tsunami modeling of a submarine landslide in the Fram Strait, *Geochem. Geophys. Geosyst.*, *10*, Q04009, doi:10.1029/2008GC002292.

1. Effects of Global Warming on the Arctic

[2] Continental margins that are influenced by glacial processes are subject to large-scale slope failures primarily at their trough mouth fans. The Norwegian Margin has experienced slope failures north of the North Sea Fan (Storegga Slide) [*Bugge et al.*, 1987; *Haflidason et al.*, 2004, 2005]. The 8.2 ka B.P. Storegga slide was associated with a very great earthquake such as the one that ruptured the whole crust over several hundred km [*Arvidsson*, 1996]. Other failures occurred at the termination of the Trænadjupet cross shelf trough (Trænadjupet Slide) [*Laberg et al.*, 2002], at the end of the Andøya cross shelf trough (Andøya Slide) [*Laberg et al.*, 2000; *Lindberg et al.*, 2004], and on the Bear Island Fan (Bear Island Slide) [*Laberg and Vorren*, 1993]. Except for the Bear Island Slide all these slope failures occurred after the last deglaciation. The reasons for these slope failures are not fully understood, but the vulnerable interlayering of glacial debris flows and hemipelagic sediments, combined with megaquake seismicity due to postglacial rebound were both probably important[*Bryn et al.*, 2005; *Kvalstad et al.*, 2005]. A vital facilitating factor for destabilizing submarine slopes appears to be development of pore water overpressure for example after gas hydrate dissociation [*Vogt and Jung*, 2002; *Micallef et al.*, 2009].

[3] In this paper we investigate what would happen if the Kongsfjorden Trough Mouth Fan (KTMF) failed. The KTMF is located in the Fram Strait on the west coast of Svalbard (Figure 1), and is one of the few trough mouth fans that have not failed since the last deglaciation.

[4] By the end of this century, average Arctic surface temperature may increase by 5°C [*Kattsov et al.*, 2004]. Climate warming is causing loss of polar ice and glacier retreat [*Rignot and Kanagaratnam*, 2006], and the reduction of ice load is already causing low-frequency earthquakes that are significantly stronger than ice flow–related earthquakes in the past [*Ekström et al.*, 2003; *Turpeinen et al.*, 2008]. Isostatic readjustment to the reduced ice load will cause the lithosphere to flex back or snap, as in the Storegga event [*Arvidsson*, 1996] potentially triggering a megaearthquake capable of setting off submarine landslides.

[5] As well as sudden events, sea-bottom warming will also destabilize gas hydrate deposits [*Westbrook et al.*, 2008b]. Similar rapid warming happened before to NW Europe at the end of the last glaciation. Gas hydrate dissociation releases free gas, increases pore pressure, and reduces effective stress and slope stability [*Sultan et al.*, 2004]. The system becomes primed for submarine slope failure, set off by a triggering earthquake. Although this mechanism is not proven so far, there is geomorphological evidence of hydrate involvement in the evolution of the Storegga Slide [*Micallef et al.*, 2009].

[6] The continental margins in the Fram Strait closely resemble the Norwegian Margin prior to the Storegga Slide (Figure 2): (1) both are characterized by an interfingering of glacial debris flow and interglacial hemipelagic sediments deposited at the mouth of a cross-shelf trough [*Vanneste et al.*, 2005], (2) both have active fluid flow systems [*Knies et al.*, 2004], (3) both are major gas hydrate provinces on the Atlantic Margin of Europe [*Westbrook et al.*, 2008a], and (4) both undergo rapid uplift as the result of postglacial rebound. In particular, the interlayering of glacial and interglacial sediments makes the slope less stable as the glacial sediments inhibit the normal dewatering of the water-rich interglacial sediments and allow pore pressure build up [*Solheim et al.*, 2005]. As a result the Svalbard glacial margin has previously failed in giant landslides such as the Hinlopen Slide 300 km northeast of the Fram Strait [*Vanneste et al.*, 2006]. The fluid flow and in particular the warming of gas hydrates add to the risk of overpressure generation in the sediments [*Sultan et al.*, 2004].

[7] The present rate of uplift in Svalbard is 4–5 mm/a [*Sato et al.*, 2006]. This is a superposition of the signal from the last glaciation and the present acceleration due to melting of ice. Similarly, 100 km^3/a ice are being lost from glaciers in Greenland and Iceland [*Luthcke et al.*, 2006]. A rebound-related earthquake has triggered the Storegga Slide [*Kvalstad et al.*, 2005] and it has been shown that earthquakes become more frequent in the Svalbard area as Greenland and Iceland adapt to the diminishing load [*Ekström et al.*, 2003].

[8] The sedimentation history and geometry, the presence of gas and the likelihood for future earthquakes as a trigger are all important prerequisites for a submarine landslide. However, whether the slope is indeed unstable also depends on the presence of weak layers, but their presence can only be established by expensive deep sea drilling. For this work we assume that these layers are

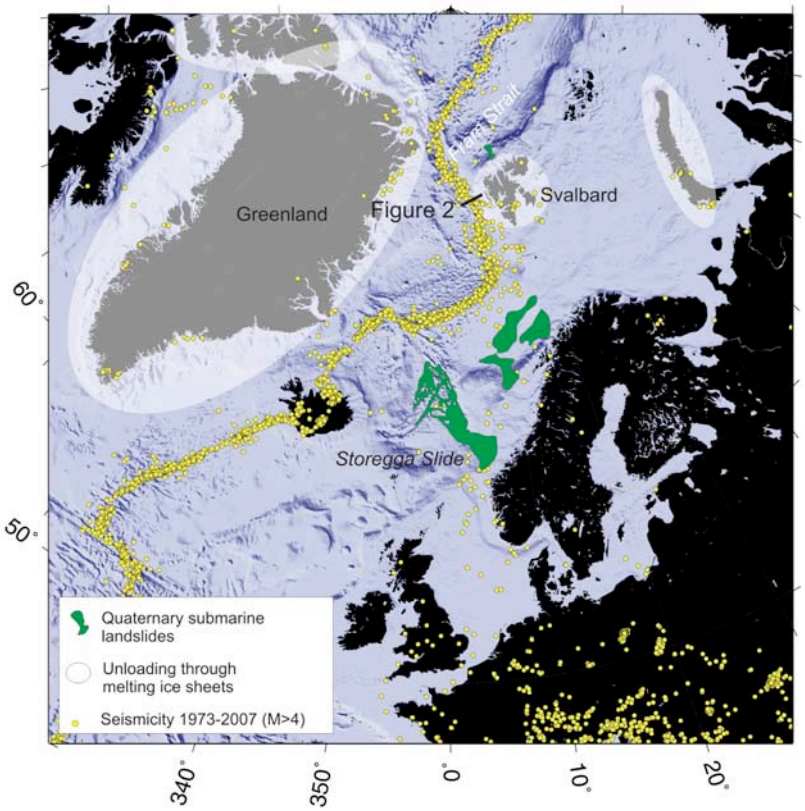

Figure 1. The Fram Strait is located between the major ice retreat areas of Greenland and Svalbard. Earthquakes occur on the rims of the ice sheets and along the mid-ocean ridges. Shaded relief based on IBCAO.

present, because they developed in many other trough mouth fans: off Hinlopen, in the Bjoernoya Fan, off Andøya, in the Trænadjupet Fan, and in the North Sea Fan. Obviously the risk for future landslides is highest for the remaining fans that have not failed yet. Current geological and geophysical data suggest that the fan off Kongsfjorden has an active fluid flow system [*Bünz et al.*, 2008; *Westbrook et al.*, 2008b] and that there is significant seismicity in the area [*Ekström et al.*, 2003]. Because such evidence is lacking for other trough mouth fans in the North Atlantic, we propose that it is the most likely site for a future failure of trough mouth fans in the North Atlantic.

[9] The part of the slope off the KTMF that could be affected by slope failure is 30 to 130 km wide in east west direction including the KTMF proper and the continental slope west of it including a continental promontory called Vestnesa. The north-south extent of a potential landslide is somewhat uncertain because the Arctic ice coverage limits the geological information available for the western side of the Yermak Plateau, but at least 130 km of

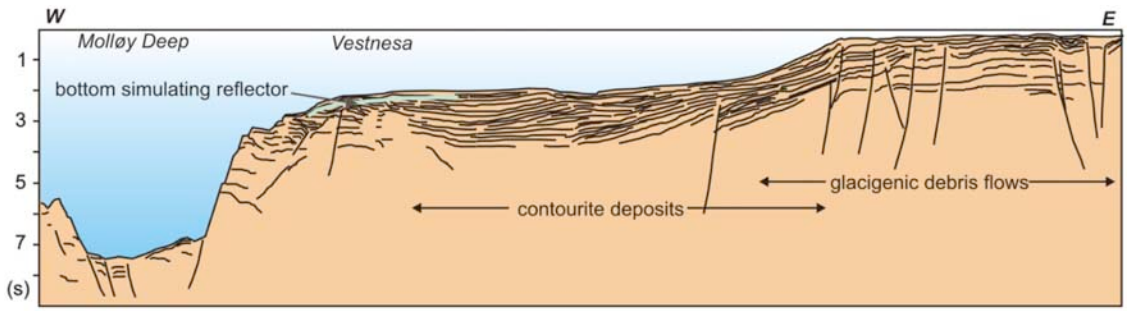

Figure 2. Line drawing of a transect from the Svalbard shelf through the gas hydrate province into the Molløy Deep [after *Eiken*, 1994].

Table 1. Key Modeling Parameters

Scenario	Volume	Lateral Dimensions	Travel Distance	Peak Speed	Maximal Froude Number	Initial Acceleration
1	500 km^3	50 × 100 km	95 km	35 m/s	0.25	0.026 m/s
2	1000 km^3	70 × 130 km	60 km	35 m/s	0.35	0.039 m/s
3	1000 km^3	70 × 130 km	60 km	20 m/s	0.2	0.013 m/s
4	1000 km^3	70 × 130 km	95 km	35 m/s	0.25	0.026 m/s

slope show a similar geological setting as the margins that were affected by the Storegga and Trænadjupet slides [*Bünz et al.*, 2008; *Westbrook et al.*, 2008b].

2. Methods and Results

2.1. Tsunami Propagation

[10] We use the finite difference, fully nonlinear Boussinesq code COULWAVE [*Lynett and Liu*, 2002] to calculate tsunami wave propagation. The change in seafloor topography due to dislocation of sediments is projected toward the sea surface. Thus the tsunami wave is build up dynamically as the slide propagates. We use North Atlantic bathymetry based on GEBCO (http://www.gebco.org), interpolated to 2.5 km bin size.

[11] We approximate the sliding body with a two-dimensional Gaussian surface. The lateral dimensions define the "Full Width at Half Maximum" values of the Gaussian package. With the landslide slopes of a Gaussian curve being very gentle, the induced water movement is considered to be solely vertical. The sediment movement itself is approximated through a kinematic slide model. We adopt a velocity profile based on *Løvholt et al.* [2005] who composed the velocity function from sinusoidal curves so that the acceleration and deceleration curves are smooth. The velocity function is composed of parts of sinusoidal curves in a way that the acceleration/deceleration curve is smooth. The velocity profile is symmetrical and the sliding stops after approximately 1 h. The shape of the velocity profile is relevant for the resulting tsunami [*Hornbach et al.*, 2007] but as there are no contradicting geological constraints available for the study area, the *Løvholt et al.* [2005] model which was calibrated against the measured runup heights of the Storegga Slide is the most appropriate analog.

[12] We model four slope failure scenarios at the Svalbard margin. Scenario 1 consists of a 500 km^3 landslide at the Svalbard slope that moves in westerly direction into the Fram Strait. It is restricted to the presently proven occurrence of gas hydrates with a 100 km long headwall and 50 km width [*Vanneste et al.*, 2005; *Westbrook et al.*, 2008b]. The slide of 100 m incision transports sediments over a distance of 95 km and stops in the Fram strait, where the slope flattens out. In scenario 2, we assume that a significant part of the slope west of Kongsfjorden is unstable. The size of this slide is based on the extent of contourite deposits on the slope as imaged by new bathymetric data [*Bünz et al.*, 2008]. It involves an area of 130 km width and 70 km length and moves in southwesterly direction. The landslide of scenario 2 mobilizes 1000 km^3 of sediments, which is still less than half of the Storegga Slide's volume [*Haflidason et al.*, 2004]. The maximal slide height is assumed again to be 100 m which is close to the Storegga Slide's 120 m [*Kvalstad et al.*, 2005] and significantly less than the Hinlopen Slide's 1400 m [*Vanneste et al.*, 2006]. The mass movement stops at a distance of 60 km downslope. In both scenarios, the maximal velocity is assumed to be 35 m/s. This celerity is based on the modeling results for Storegga [*Løvholt et al.*, 2005], which we assume to be a good analog for the sediment properties off Svalbard. The shape of the slide will also have an effect on the resultant tsunami [*Ward*, 2001], but as there are no further constraints on this we assume oval shaped slides which will result in average tsunami parameters.

[13] Exact parameters of an event are hard to predict. So, scenario 3 and 4 include variations of the important parameters volume, celerity and initial acceleration. Scenario 3 is similar to scenario 2, the difference lies in the maximal slide speed only. Scenario 4 uses the location and dynamical properties of scenario 1, while moving twice as much sediment volume. The parameters for each scenario are listed in Table 1.

2.2. Modeling Results

[14] The maximum wave height distributions of each scenario are presented together with the slide form in Figures 3a, 3b, 4a, and 5a. While the wave

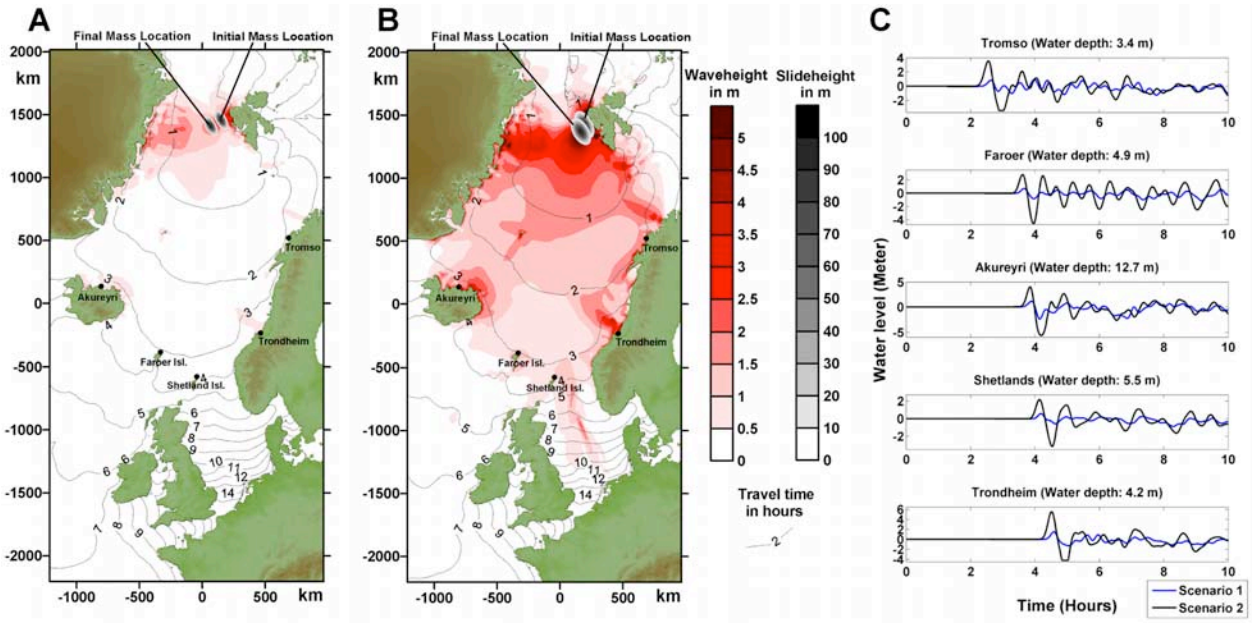

Figure 3. (a and b) Slide location, maximal wave elevation, and arrival times for scenarios 1 and 2, respectively. (c) Synthetic tide gauge measurements at indicated locations and water depths. If receding waves exceed gauge depths, the tide gauges saturate and water level history is recorded as negative water depth. Time series start at the beginning of the slide movement.

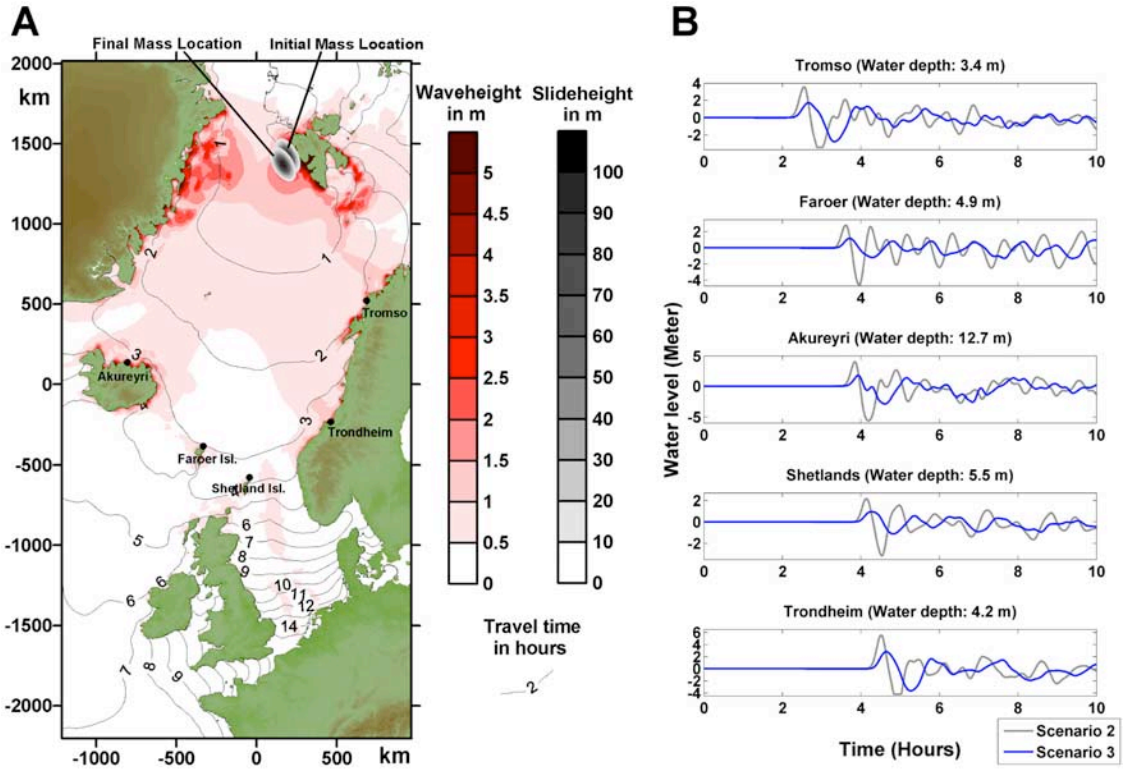

Figure 4. (a) Slide location, maximal wave elevation, and arrival times for scenario 3. (b) Mareogram comparison between scenarios 2 (35 m/s maximal velocity) and 3 (20 m/s).

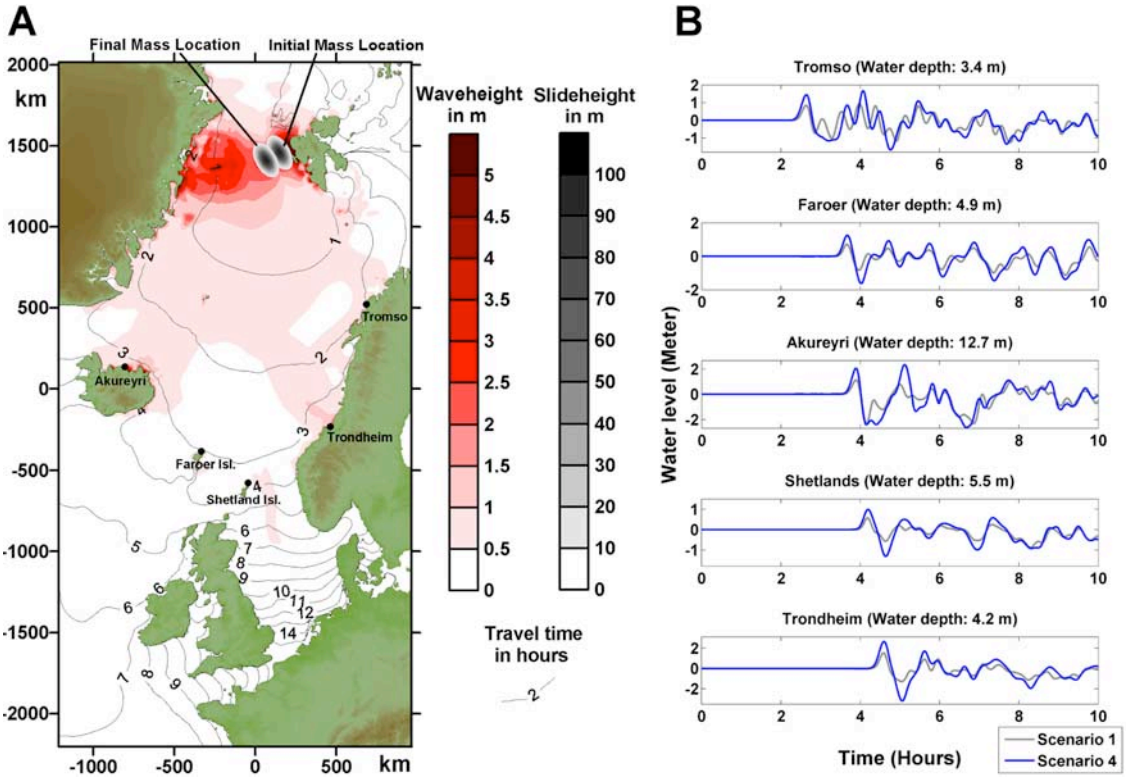

Figure 5. (a) Scenario 4 slide location, maximal wave elevation, and arrival times. (b) Mareogram comparison between scenario 1 (500 km^3 volume) and scenario 4 (1000 km^3), where all other parameters are identical.

heights of scenario 1 are small, scenario 2 generates a large tsunami. Tsunami heights are calculated for cities on the Norwegian coast, the Faroe and Shetland islands, and Iceland. In this context it must be noted that actual runup depends strongly on local topography [*Hornbach et al.*, 2008], especially in fjords and can be significantly smaller or larger than the computed maximal wave heights. Mareograms for selected locations are depicted in Figure 3c. The results show waves up to 6 m. Although the Norwegian Sea coasts are rocky and population densities are low, it is clear that a tsunami of this size would cause significant damage to communities in eastern Greenland, Norway and Iceland.

[15] The comparison of scenario 2 and 3 (Figure 4b) shows the influence of the slide speed. By decreasing the maximum slide velocity from 35 m/s to 20 m/s, wave heights lower by a factor of more than two (Table 2). This nonlinear dependence can be explained by describing the buildup phase of the wave. If the slide moves much slower than the water waves, the slide-induced uplift of the water surface levels quickly. For fast slides, the uplift of each time step superposes onto the wave, increasing its height significantly. Therefore, the ratio of wave velocity to slide speed, termed Froude number, can be regarded as a measure for the effectiveness in tsunami excitation of a slide (Table 1 and *Ward* [2001]). The control of slide volume on a tsunami can be seen by comparing scenario 1 and 4 (Figure 5b and Table 2). An increase of the volume by a factor of two doubles

Table 2. Maximal Wave Heights

Scenario	Tromsø (Depth 3.4 m)	Faroer (Depth 4.9 m)	Akureyri (Depth 12.7 m)	Shetlands (Depth 5.5 m)	Trondheim (Depth 4.2 m)
1	0.9 m	0.7 m	1.1 m	0.6 m	1.5 m
2	3.6 m	2.8 m	4.0 m	2.2 m	5.6 m
3	1.7 m	1.2 m	1.8 m	1.0 m	2.8 m
4	1.7 m	1.3 m	2.4 m	1.0 m	2.6 m

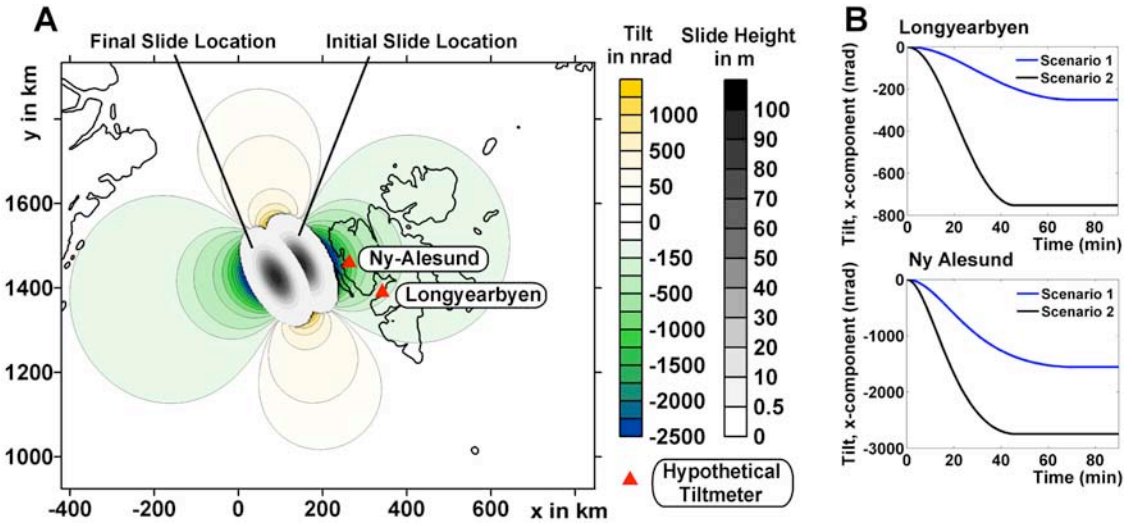

Figure 6. (a) Surface tilting in x direction for landslide of scenario 1. (b) X component of theoretical tiltmeter measurements. For typical errors of 100 nrad, scenarios 1 and 2 are clearly distinguishable.

the resultant maximum wave heights, indicating a linear dependency within this parameter range.

[16] The slide direction strongly influences the wave radiation pattern. The scenarios 1 and 4 with a westward slide direction radiate a significant part of the energy toward Greenland, leaving northwest Europe with relatively small wave amplitudes. A slide moving toward southwest (scenarios 2 and 3), however, releases the leading wave energy directly into the Norwegian Sea. Although the basin topography has a defocusing effect on the tsunami, the wave heights in northwest Europe double compared to the slides in westward direction. Unfortunately, the general southwesterly dip direction of the Svalbard margin between Prins Karl Forlandet and Vestnesa make a southwesterly direction for the slide more likely than a westerly direction.

3. Implications for a Tsunami Warning System

[17] With respect to the impact on coastal communities, a tsunami warning facility would be worthwhile. Unfortunately, predicted surface displacements (around 10 cm, maximum) can be only marginally detected by real-time GPS observations. Thus, the otherwise very efficient tsunami warning technique based on near-field GPS observations [*Sobolev et al.*, 2007] is not suitable in this case. We propose a new tool for Landslide Tsunami Early Warning. The method is based on the fact that a mass displacement of $\sim 10^{15}$ kg will lead to a notable surface deformation. Following the assumption of the elastic half-space, we estimate the amount of surface tilting using an analytical solution [*Melchior*, 1966].

$$\alpha_{1,2} = \frac{\partial u_3}{\partial x_{1,2}}$$

$$u_3 = -\left[\frac{1-\nu}{2\pi G} + \frac{f}{g^2}\right]\Phi$$

$$\Phi = \iint \frac{P(\varsigma_1, \varsigma_2)}{R(x_1, x_2, 0, \varsigma_1, \varsigma_2)} d\varsigma_1 d\varsigma_2$$

$$R(x_1, x_2, 0, \varsigma_1, \varsigma_2) = \left[(x_1 - \varsigma_1)^2 + (x_2 - \varsigma_2)^2\right]^{1/2}$$

These formulas allow to calculate the tilt signal in x and y direction ($\boldsymbol{\alpha_{1,2}}$) due to a load distribution ($\boldsymbol{P}$). We apply it to the initial and the final sediment distribution. The measurable change in surface tilt during the landslide is computed as the difference between final and initial tilt signal. Further involved variables and parameter are as follows: $\boldsymbol{u_3}$, vertical displacement (z axis directed upward); $\mathbf{x_{1,2}}$, point of observation; $\boldsymbol{\zeta_{1,2}}$, point of load; $\boldsymbol{R}$, distance; $\boldsymbol{f}$, gravitational constant ($6.67 \cdot 10^{-11}$ $\mathrm{Nm^2\ kg^{-2}}$); $\boldsymbol{g}$, standard gravity ($9.81\ \mathrm{ms^{-2}}$); ν, Poisson ratio (0.25); $\boldsymbol{G}$, shear modulus ($7 \cdot 10^{10}$ Pa).

[18] As the deformation due to the slide involves large lithospheric portions, the involved parameters of the elastic half-space are evaluated at lithospheric depths: The Poisson ratio of 0.25 is a lithospheric average and the value of the Shear Modulus is estimated at a depth of 100 km which corresponds to the distance between tiltmeter and load. We implement biaxial tiltmeters. One leg measures tilts

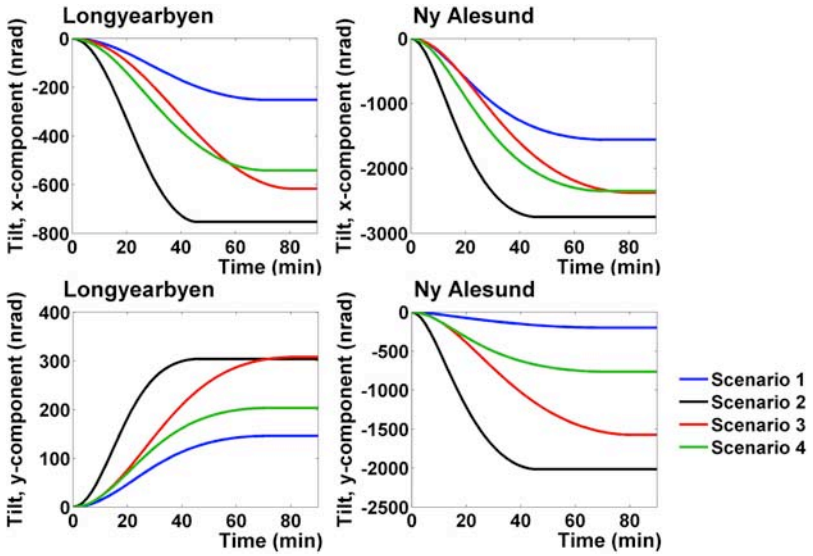

Figure 7. Hypothetical tiltmeter measurements. Shown are x and y components of each scenario.

in positive x direction (east), the other in positive y direction (north).

[19] The overall tilt distribution for the x component is depicted in Figure 6a. Tilt measurements of hypothetical inclinometers positioned at Longyearbyen and Ny-Ålesund are shown in Figure 6b. Occurring tilt amplitudes of the order of 1000 nrad are extremely well within the accuracy range of several nanorad for today's tiltmeters [*d'Oreye and Zürn*, 2005].

[20] For each of the four scenarios, Figure 7 depicts the components of the computed tilt vector in x and y direction. The time series of the x components for scenario 3 and 4 are very similar, however, they can be distinctly discriminated via the y component. Within these possible events, the most hazardous scenario 2 can be clearly recognized.

[21] By implementing inclinometers at Spitsbergen, a large submarine mass movement can be reliably detected a few minutes after slide initiation. We envisage a setup in which the tiltmeter response and the range of likely tsunamis is modeled for several realistic landslide scenarios before installation of the tiltmeters. In this case tsunami-relevant parameters like displaced mass, travel distance and velocity will be accessible as soon as the bulk of the mass has moved, i.e., approximately after 1 h. Obviously slow precursors or runout of turbidites may occur over a longer time span, but as the tsunami is linked to the main acceleration of the bulk of the landslide only this information is necessary for the tsunami warning system (Figure 6b).

4. Conclusions

[22] From modeling different tsunami scenarios we conclude that a landslide in the Fram Strait has the potential to create a tsunami that would affect NW Europe. Present global warming increases the probability for such an event. We calculate the effect that such an event would have on tiltmeters and conclude that the installation of such instruments on the west coast off Svalbard would be an efficient warning tool that gives several hours of advance warning before a tsunami would strike the coasts of Norway, Iceland and the UK.

Acknowledgments

[23] We wish to thank Patrick Lynett for providing COULWAVE and the kind introduction to its use. The insightful comments of two anonymous reviewers improved the manuscript.

References

Arvidsson, R. (1996), Fennoscandian earthquakes: Whole crustal rupturing related to postglacial rebound, *Science*, *274*(5288), 744–746, doi:10.1126/science.1274.5288.1744.

Bryn, P., et al. (2005), Explaining the Storegga Slide, *Mar. Pet. Geol.*, *22*(1–2), 11–19, doi:10.1016/j.marpetgeo.2004.12.003.

Bugge, T., et al. (1987), A giant three-stage submarine slide off Norway, *Geo Mar. Lett.*, *7*, 191–198, doi:10.1007/BF02242771.

Bünz, S., et al. (2008), Environmentally sensitive gas hydrates on the W-Svalbard margin at the gateway to the Arctic

Ocean, paper presented at 6th International Conference on Gas Hydrates, Chevron, Vancouver, B. C., Canada, 6–10 July 2008.

d'Oreye, N. F., and W. Zürn (2005), Very high resolution long-baseline water-tube tiltmeter 265 to record small signals from Earth free oscillations up to secular tilts, *Rev. Sci. Instrum.*, *76*, 024501, doi:10.1063/1.1844451.

Eiken, O. (Ed.) (1994), Seismic atlas of western Svalbard, *Medd. 130*, Norsk Polar Inst., Oslo.

Ekström, G., et al. (2003), Glacial earthquakes, *Science*, *302*(5645), 622–624, doi:10.1126/science.1088057.

Haflidason, H., et al. (2004), The Storegga Slide: Architecture, geometry and slide-development, *Mar. Geol.*, *213*, 201–234, doi:10.1016/j.margeo.2004.10.007.

Haflidason, H., et al. (2005), The dating and morphometry of the Storegga Slide, *Mar. Pet. Geol.*, *22*(1–2), 123–136, doi:10.1016/j.marpetgeo.2004.10.008.

Hornbach, M. J., et al. (2007), Triggering mechanism and tsunamogenic potential of the Cape Fear Slide complex, U.S. Atlantic margin, *Geochem. Geophys. Geosyst.*, *8*, Q12008, doi:10.1029/2007GC001722.

Hornbach, M. J., et al. (2008), Did a submarine slide trigger the 1918 Puerto Rico tsunami?, *Sci.Tsunami Hazards*, *27*(2), 22–31.

Kattsov, V. M., et al. (2004), Future climate change: Modeling and scenarios for the Arctic, in *Arctic Climate Impact Assessment*, edited by S. J. Hassol, pp. 99–150, Cambridge Univ. Press, Cambridge, U. K.

Knies, J., et al. (2004), Near-surface hydrocarbon anomalies in shelf sediments off Spitsbergen: Evidences for past seepages, *Geochem. Geophys. Geosyst.*, *5*, Q06003, doi:10.1029/2003GC000687.

Kvalstad, T. J., et al. (2005), The Storegga slide: Evaluation of triggering sources and slide mechanics, *Mar. Pet. Geol.*, *22*(1–2), 245–256, doi:10.1016/j.marpetgeo.2004.10.019.

Laberg, J. S., and T. O. Vorren (1993), A Late Pleistocene submarine slide on the Bear Island Trough Mouth Fan, *Geo Mar. Lett.*, *13*, 227–234, doi:10.1007/BF01207752.

Laberg, J. S., et al. (2000), The Andøya Slide and the Andøya Canyon, north-eastern Norwegian-Greenland Sea, *Mar. Geol.*, *162*, 259–275, doi:10.1016/S0025-3227(99)00087-0.

Laberg, J. S., T. Vorren, J. Mienert, P. Bryn, and R. Lien (2002), The Trænadjupet Slide: A large slope failure affecting the continental margin of Norway 4,000 years ago, *Geo Mar. Lett.*, *22*, 19–24.

Lindberg, B., et al. (2004), The Nyk Slide—Morphology, progression, and age of a partly buried submarine slide offshore northern Norway, *Mar. Geol.*, *213*(1–4), 277–289, doi:10.1016/j.margeo.2004.10.010.

Løvholt, F., et al. (2005), A parametric study of tsunamis generated by submarine slides in the Ormen Lange/Storegga area off western Norway, *Mar. Pet. Geol.*, *22*(1–2), 219–231, doi:10.1016/j.marpetgeo.2004.10.017.

Luthcke, S. B., et al. (2006), Recent Greenland ice mass loss by drainage system from satellite gravity observations, *Science*, *314*(5803), 1286–1289, doi:10.1126/science.1130776.

Lynett, P., and P. L.-F. Liu (2002), A numerical study of submarine-landslide-generated waves and run-up, *Philos. Trans. R. Soc. A*, *458*, 2885–2910, doi:10.1098/rspa.2002.0973.

Melchior, P. (1966), *The Earth Tides*, Pergamon, Oxford, U. K.

Micallef, A., D. G. Masson, C. Berndt, and D. A. V. Stow (2009), Development and mass movement processes of the north-eastern Storegga Slide, *Quat. Sci. Rev.*, *28*(5–6), 433–448.

Rignot, E., and P. Kanagaratnam (2006), Changes in the velocity structure of the Greenland Ice Sheet, *Science*, *311*, 986–990, doi:10.1126/science.1121381.

Sato, T., et al. (2006), A geophysical interpretation of the secular displacement and gravity rates observed at Ny-Ålesund, Svalbard in the Arctic; effects of post-glacial rebound and present-day ice melting, *Geophys. J. Int.*, *165*(3), 729–743, doi:10.1111/j.1365-246X.2006.02992.x.

Sobolev, S. V., et al. (2007), Tsunami early warning using GPS-Shield arrays, *J. Geophys. Res.*, *112*, B08415, doi:10.1029/2006JB004640.

Solheim, A., et al. (2005), The Storegga Slide complex: Repetitive large scale sliding with similar cause and development, *Mar. Pet. Geol.*, *22*(1–2), 97–107, doi:10.1016/j.marpetgeo.2004.10.013.

Sultan, N., et al. (2004), Effect of gas hydrate melting on seafloor slope instability, *Mar. Geol.*, *213*(1–4), 379–401, doi:10.1016/j.margeo.2004.10.015.

Turpeinen, H., et al. (2008), Effect of ice sheet growth and melting on the slip evolution of thrust faults, *Earth Planet. Sci. Lett.*, *269*(1–2), 230–241, doi:10.1016/j.epsl.2008.1002.1017.

Vanneste, M., et al. (2005), Bottom-simulating reflections and geothermal gradients across the western Svalbard margin, *Terra Nova*, *17*(6), 510–516, doi:10.1111/j.1365-3121.2005.00643.x.

Vanneste, M., et al. (2006), The Hinlopen Slide: A giant, submarine slope failure on the northern Svalbard margin, Arctic Ocean, *Earth Planet. Sci. Lett.*, *245*(1–2), 373–388, doi:10.1016/j.epsl.2006.02.045.

Vogt, P. R., and W.-Y. Jung (2002), Holocene mass wasting on upper non-Polar continental slopes—Due to post-Glacial ocean warming and hydrate dissociation?, *Geophys. Res. Lett.*, *29*(9), 1341, doi:10.1029/2001GL013488.

Ward, S. N. (2001), Landslide tsunami, *J. Geophys. Res.*, *106*(B6), 11,201–11,215, doi:10.1029/2000JB900450.

Westbrook, G. K., et al. (2008a), Active gas venting at the landward limit of hydrate stability offshore Svalbard, *Eos Trans. AGU*, *89*(53), Fall Meet. Suppl., Abstract OS31D-03.

Westbrook, G. K., et al. (2008b), Estimation of gas hydrate concentration from multi-component seismic data at sites on the continental margins of NW Svalbard and the Storegga region of Norway, *Mar. Pet. Geol.*, *25*(8), 744–758, doi:10.1016/j.marpetgeo.2008.02.003.